Available online at www.sciencedirect.com
SCIENCE DIRECT®
Journal of Solid State Chemistry 177 (2004) 1258–1267
JOURNAL OF SOLID STATE CHEMISTRY
http://elsevier.com/locate/jssc

Crystal structure of an open-tunnel oxide α-MnO_2 analyzed by Rietveld refinements and MEM-based pattern fitting

Norihito Kijima,[a,*] Takuji Ikeda,[b,1] Kenichi Oikawa,[c,2] Fujio Izumi,[b] and Yuji Yoshimura[a]

[a] *National Institute of Advanced Industrial Science and Technology, Tsukuba Central 5, 1-1-1 Higashi, Tsukuba, Ibaraki 305-8565, Japan*
[b] *Advanced Materials Laboratory, National Institute for Materials Science, 1-1 Namiki, Tsukuba, Ibaraki 305-0044, Japan*
[c] *Advanced Science Research Center, Japan Atomic Energy Research Institute, Tokai, Naka, Ibaraki 319-1195, Japan*

Received 11 June 2003; received in revised form 12 October 2003; accepted 29 October 2003

Abstract

The crystal structure of an open-tunnel oxide, α-MnO_2, free from any large stabilizing cations was analyzed by Rietveld refinement and whole-pattern fitting based on the maximum-entropy method (MEM). Rietveld refinement from neutron powder diffraction data for a partially deuterated specimen of $MnO_2 \cdot 0.1(D_{0.34}H_{0.66})_2O$ showed it to have a hollandite-type structure (tetragonal; space group $I4/m$; $a = 9.777(2)$ and $c = 2.8548(5)$ Å; $Z = 8$; $R_{wp} = 4.56\%$, $R_p = 3.67\%$, $R_B = 1.52\%$, and $R_F = 0.77\%$; $S = 1.23$). The bond valence sum of Mn was calculated at +4.04. The quadratic elongation and bond angle variance for the MnO_6 octahedron proved that its distortion is relatively small even if small H_2O molecules are contained in tunnels instead of large stabilizing cations. Electron-density distribution (EDD) in $MnO_2 \cdot 0.15H_2O$ was visualized by MEM-based pattern fitting from both synchrotron and conventional X-ray powder diffraction data. The resulting EDD images showed that the inner effective diameters of a cage in α-MnO_2 are about 2.6 Å for a bottleneck on the (002) plane and about 4.8 Å for an inner space on the (001) plane. Thus, H_2O molecules (2.2 Å) can be trapped in the narrow tunnels of α-MnO_2, whereas N_2 molecules (4.3 Å) cannot penetrate the tunnel cavity. Elongation of electron densities for tunnel water along the tunnel direction was observed in the EDD images. Further, to obtain a reasonable isotropic atomic displacement parameter for the O3 site in the tunnel cavity, O3 had to be split into two pieces at the 4*e* site in the Rietveld refinement from the neutron diffraction data. These findings provide evidence that H_2O molecules are not only vibrating markedly but also highly disordered, particularly along the [001] direction, near the center of the cage.

Keywords: α-MnO_2; Hollandite-type structure; Neutron powder diffraction; X-ray powder diffraction; Rietveld analysis; Maximum-entropy method; Electron-density distribution

1. Introduction

Even nowadays, structure refinements of porous and layered manganese oxides are not straightforward. Although these manganese oxides have been extensively studied for the past few decades, details in many of their crystal structures are poorly understood, and basic crystal structures of several phases remain unknown. In most cases, the main difficulty exists in the lack of crystals suitable for single-crystal X-ray diffraction experiments. In the past few years, however, Rietveld refinements [1–3] from X-ray and neutron powder diffraction data have provided important new insights into the crystal structures of some manganese oxides [4].

Several manganese oxides with tunnel structures have been synthesized so far [4–8]. α-MnO_2 has a hollandite-type structure (space group $I4/m$, No. 87) comprising double chains of MnO_6 octahedra forming (2×2) tunnels. At present, only α-MnO_2 is known to have a tunnel structure without any large stabilizing cations in its tunnel cavity, whereas the other porous manganese oxides, e.g., romanechite (2×3) and todorokite (3×3), contain some large stabilizing cations in their tunnels. This open-tunnel oxide, α-MnO_2, is an attractive material for various industrial applications such as an insertion electrode for lithium-ion secondary batteries

*Corresponding author.
E-mail address: n-kijima@aist.go.jp (N. Kijima).
[1] Present address: National Institute of Advanced Industrial Science and Technology, 4-2-1 Nigatake, Miyagino-ku, Sendai, Miyagi 983-8551, Japan.
[2] Present address: Center for Proton Accelerator Facility, Japan Atomic Energy Research Institute, Tokai, Naka, Ibaraki 319-1195, Japan.

0022-4596/$ - see front matter © 2003 Elsevier Inc. All rights reserved.
doi:10.1016/j.jssc.2003.10.038

[6], an ion- or molecular-sieve [7], a catalyst [8], and a host material for a one-dimensional superionic conductor [9,10].

In 1950, Byström and Byström [11] at first determined the crystal structures of hollandite minerals from a Swedish manganese ore from single-crystal X-ray diffraction data taken with a Weissenberg camera. They found that hollandite was essentially tetragonal ($I4/m$) and in some cases distorted to be monoclinic ($I2/m$). Later, Post et al. [12] refined structure parameters of three hollandite minerals and discussed distributions of tunnel ions. Thereafter, they intensively studied the crystal structures of several porous and layered manganese oxides by the Rietveld method [13–16]. In 1992, Rossouw et al. [17] successfully synthesized polycrystalline α-MnO_2 free from any large stabilizing cations in its tunnels and carried out Rietveld refinements from neutron diffraction data of hydrated and dehydrated α-MnO_2 specimens. Difference Fourier synthesis suggested that H_2O molecules (or H_3O^+ ions) partially occupy the tunnel cavity. However, the nature and locations of the residual H_2O molecules in its tunnels remain unclear at present.

Various methods have been used to prepare α-MnO_2, having significant influences on the properties of the products. We have recently succeeded in synthesizing a high-purity and well-crystallized specimen of α-MnO_2 free from any large stabilizing cations in its tunnel cavity by a precipitation method using ozone oxidation [18]. In our synthetic method, α-MnO_2 can directly be formed in solutions containing no cations other than Mn^{2+}. Therefore, our specimen does not contain any cationic residues such as Li^+, K^+, and Ba^{2+} ions in the tunnels.

In the porous manganese oxides, α-MnO_2 is the only compound that does not contain any large stabilizing cations in its tunnel cavity. Neither this open tunnel structure nor a state of residual H_2O molecules in its tunnel cavity has been understood well. To clarify the structural properties of α-MnO_2 including H_2O molecules in its tunnel, we have refined its structure parameters by Rietveld analysis from neutron, synchrotron X-ray, and conventional X-ray powder diffraction data of a $MnO_2 \cdot nH_2O$ specimen prepared by the ozone-oxidation method. Furthermore, we have visualized electron-density distribution (EDD) in $MnO_2 \cdot nH_2O$ by whole-pattern fitting based on the maximum-entropy method (MEM) [19–21]. EDD determined in this way is expected to provide us with valuable information on the residual H_2O molecules in the tunnel cavity.

We report here the crystal data of α-MnO_2 including H_2O molecules in its tunnel cavity and EDD in it. We also discuss its framework structure and the positional disorder and thermal motion of the residual H_2O molecules in its tunnel cavity. The results presented below will be fruitful enough to understand the detailed structural properties of α-MnO_2.

2. Experimental

2.1. Sample preparation

$MnO_2 \cdot nH_2O$ was prepared by the precipitation method using ozone oxidation [18]. Fourteen grams of $MnSO_4 \cdot 5H_2O$ (99.9%, Wako Pure Chemical Ind. Ltd.) was dissolved in 600 cm^3 of a 3 mol/dm^3 solution of H_2SO_4; subsequently, this solution was heated up to 80°C while being stirred at 200 rpm. The solution was bubbled by a mixture of O_3 and O_2, where O_2 was partially changed into O_3 with an ozonizer. The rate of flowing the gas mixture was 40 cm^3/min while the concentration of O_3 was 135 mg/dm^3. After bubbling the gas for 3 h, the product was filtered off and washed with deionized water until washings were practically free from H_2SO_4. It was then freeze-dried in an evacuated bottle for about 10 h using a freeze-dryer. Scanning electron microscopy (SEM) and transmission electron microscopy (TEM) images of the $MnO_2 \cdot nH_2O$ specimen showed that surfaces of particles were covered almost uniformly with needle crystals which were elongated parallel to the c-axis, i.e., along the direction of the tunnel (Fig. 1). Details of the preparation and characterization of $MnO_2 \cdot nH_2O$ were reported in the previous work [18].

2.2. Compositional analyses

The hydrogen content in the specimen was determined by combustion analysis using an elemental analyzer. The manganese content was analyzed by inductively coupled plasma-atomic emission spectroscopy. The H/Mn amount-of-substance ratio was determined by the above elemental analyses. The oxygen content was analyzed by a titration method in what follows. The sample (about 0.1 g) was dissolved in 10 cm^3 of an $H_2C_2O_4$ solution (0.5 mol/dm^3) and 10 cm^3 of an H_2SO_4 solution (0.5 mol/dm^3) to reduce all the Mn^{n+} ($n>2$) ions to Mn^{2+} ions. The excess amount of $C_2O_4^{2-}$ ions in the solution was determined by titration at around 60°C with a standard solution of $KMnO_4$ (0.02 mol/dm^3, Wako Pure Chemical Ind., Ltd.) The resultant chemical composition of the specimen was $H_{0.48}MnO_{2.23}$, which affords a mean oxidation state of Mn, +3.98.

Prior to a neutron diffraction experiment, $MnO_2 \cdot nH_2O$ was partially deuterated to minimize incoherent scattering by H. After the specimen had been kept in D_2O at 70°C for 3 d, it was dried in an evacuated bottle at room temperature. The D:H amount-of-substance ratio was measured by temperature-programmed-desorption (TPD) analysis on a quadruple mass spectrometer. The specimen was heated from 25°C to 800°C at a linear heating rate of 5°C/min in a flowing mixture of O_2 (50 cm^3/min) and N_2 (200 cm^3/min). The amounts of desorbed gases were calculated from peak areas for

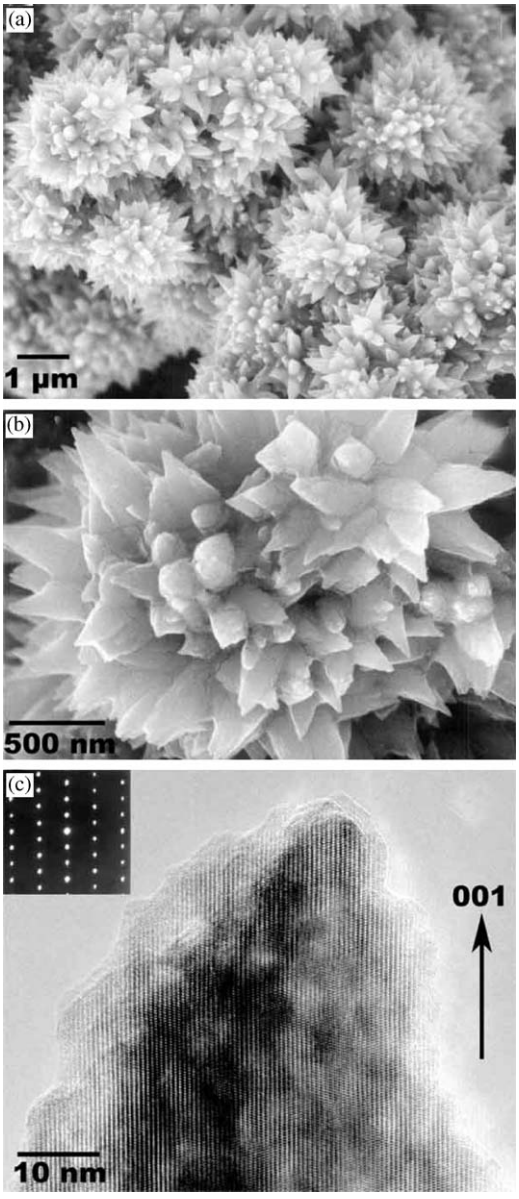

Fig. 1. (a), (b) Scanning electron microscopy and (c) transmission electron microscopy images of $MnO_2 \cdot nH_2O$.

H_2O, HDO, and D_2O. The D:H amount-of-substance ratio was estimated to be 0.34:0.66 from the amounts of the desorbed gases; this ratio was fixed on introduction of a virtual chemical species into Rietveld refinements described later.

The amounts of H_2O adsorbed and occluded within the tunnel of α-MnO_2 were determined by thermogravimetry (TG) and TPD analysis. The TPD profile for H_2O could be decomposed into two peaks associated with adsorbed and tunnel water [18]. From the peak area at higher temperature, the amount of H_2O occluded within the tunnels was estimated to be about 0.1 mol per mol of MnO_2.

2.3. Diffraction experiments

Neutron powder diffraction data were measured at room temperature on the high-resolution powder diffractometer HRPD at the JRR-3M reactor. The specimen deuterated was contained in a cylindrical vanadium cell with an inner diameter of 12 mm. The neutron wavelength was 1.1635 Å, and the neutron diffraction data were collected between $2\theta = 5°$–$165°$ with a step interval of 0.05°.

Synchrotron X-ray powder diffraction (XRD) data were collected at room temperature on the high-resolution powder diffractometer at beam line BL15XU of SPring-8 with the Debye–Scherrer geometry using a Ge (111) analyzer. The specimen was loaded into a quartz-glass capillary tube with an inner diameter 0.3 mm; this capillary tube was rotated at a speed of 60 rpm during the measurement to minimize a preferred-orientation effect. The XRD data were measured between $2\theta = 5°$–$80°$ with a wavelength of 0.9997 Å and a step interval of 0.02°.

XRD data were also taken with Cu$K\alpha$ radiation at room temperature on a Bragg–Brentano-type powder diffractometer (MAC science MXP-18VTZ) with a vertical θ–θ geometry. These data will be referred to as conventional XRD data here. To suppress axial divergence and make diffraction profiles in the low-2θ region as symmetric as possible, its goniometer was equipped with a pair of long horizontal Soller slits to decrease the angular aperture to 1°. Moreover, the goniometer was provided with variable-width divergence and scattering slits to improve counting statistics in the high-2θ region by fixing the irradiation width at 20 mm and to suppress the background level in the low-2θ region, respectively. The specimen crushed sufficiently was charged into a flat glass holder 5 mm in thickness to keep the absorption factor constant regardless of 2θ. The XRD data were measured in a 2θ range from 10° to 120° with a step interval of 0.03°.

2.4. Procedures of structure refinements

The diffraction data were analyzed by the Rietveld method with RIETAN-2000 [19–23] on the basis of space group $I4/m$. A split pseudo-Voigt profile function formulated by Toraya [24] was used in all the refinements; the technique of partial profile relaxation [19,22] was applied to (nearly) isolated reflections whose profiles were anisotropically broadened. The structure refinements were carried out by following the ''Rietveld refinement guidelines'' [25]. Table 1 lists other details in the Rietveld refinements.

EDD in $MnO_2 \cdot nH_2O$ was visualized by MEM-based pattern fitting (MPF) [19–21]. When dealing with powder diffraction data having heavily overlapping reflections, integrated intensities are often estimated on

Table 1
Crystallographic data and details in the data collection and structure refinements[a]

Radiation	Neutron	Synchrotron X-ray	Conventional X-ray
Chemical formula	$MnO_2 \cdot 0.1(D_{0.34}H_{0.66})_2O$	$MnO_2 \cdot 0.15H_2O$	$MnO_2 \cdot 0.15H_2O$
Crystal system	tetragonal	tetragonal	tetragonal
Space group	$I4/m$	$I4/m$	$I4/m$
Z	8	8	8
a (Å)	9.777(2)	9.81359(10)	9.82304(12)
c (Å)	2.8548(5)	2.85077(2)	2.85474(3)
V (Å^3)	272.89(8)	274.548(4)	275.459(5)
R_{wp} (%)	4.56[b]	2.66[b] 2.53[c]	5.06[b] 4.38[c]
R_e (%)	3.70[b]	1.61[b] 1.59[c]	3.41[b] 3.38[c]
R_p (%)	3.67[b]	2.02[b] 1.91[c]	3.76[b] 3.13[c]
R_B (%)	1.52[b]	3.02[b] 1.19[c]	3.16[b] 0.72[c]
R_F (%)	0.77[b]	1.52[b] 0.79[c]	1.41[b] 0.51[c]
S	1.23[b]	1.66[b] 1.59[c]	1.48[b] 1.30[c]
Wavelength (Å)	1.1635	0.9997	1.5418
2θ range (deg)	5–165	5–80	10–120
2θ step width (deg)	0.05	0.02	0.03
Number of reflections	417	196	132
Number of relaxed reflections	10	26	18

[a] The R factors and S are defined in Ref. [28]. Numbers in parentheses give the estimated standard deviations of the last significant digit.
[b] After Rietveld refinement.
[c] After two REMEDY cycles.

the basis of the result of Rietveld analysis. To minimize the bias imposed on electron densities by the structure model in the Rietveld analysis, the following iterative procedure of MPF was carried out. After the Rietveld refinement with RIETAN-2000, independent 'observed' structure factors, F_o (Rietveld), were estimated from the XRD data on the basis of refined parameters [1]. The resulting F_o (Rietveld) data were analyzed by an MEM-analysis program PRIMA [21]. In the MEM analysis, the unit cell was divided into $128 \times 128 \times 48$ pixels with the number of electrons in the unit cell, i.e., $F(000)$, fixed at 340. In the subsequent whole-pattern fitting (w.p.f.), structure factors were fixed at F_c (MEM)'s obtained by the MEM analysis, while the scale factor and lattice, profile, peak-shift, and background parameters were refined by a least-squares method with RIETAN-2000. F_o (w.p.f.)'s reevaluated after the whole-pattern fitting were analyzed again with PRIMA. Whole-pattern fitting and MEM analysis were alternately repeated in the above way (REMEDY cycles) until R factors in the former no longer decrease practically.

Two-dimensional EDD maps of $MnO_2 \cdot nH_2O$ were plotted with MEVIUS developed by Kumazawa, and three-dimensional EDD and crystal-structure models were visualized with VEND and VICS [21,26], respectively.

3. Structure refinements

3.1. Rietveld analysis from the Neutron diffraction data

All the reflections were indexed on the basis of tetragonal symmetry with space group $I4/m$. Bound coherent-scattering lengths, b_c, used for the Rietveld refinement adopting $I4/m$ were -3.750 fm for Mn, 5.803 fm for O, -3.739 fm for H, and 6.671 fm for D [27]. Anisotropic atomic displacement parameters, U_{ij}, were assigned to each site except for tunnel water. The technique of partial profile relaxation [19,22] was applied to 10 reflections with profiles broadened anisotropically.

We first tried to refine structure parameters of O and D/H sites for tunnel water independently, but their occupancies, g, and isotropic atomic displacement parameters, U, could not be refined simultaneously. They diverged to extraordinarily large values; an unreasonably large O–D/H distance was obtained in comparison with that in water. This result is attributed to the fact that D/H sites are practically transparent in this specimen because b_c for the D/H species is calculated at -0.1996 fm ($= 6.671 \times 0.34 - 3.739 \times 0.66$ fm) from the D:H amount-of-substance ratio determined by the TPD analysis. We therefore neglected D/H atoms and refined only the structure parameters of an O3 site in the tunnel cavity.

We then assigned the $2b$ $(0, 0, 1/2)$ site to O3. Because of strong correlations among g(O3) and U_{ij}(O3)'s, g(O3) was fixed at the value analyzed by TG and TPD. As this stage, the equivalent isotropic atomic displacement parameter, U_{eq}(O3), was 0.160 Å^2 which is unreasonably large even considering marked thermal motion of small and neutral H_2O molecules in the tunnel cavity. These findings offer evidence for the pronounced positional disorder of H_2O molecules in the tunnel cavity. U_{33}(O3) was more than twice as large as U_{11}(O3), which must reflect more pronounced static disorder along the tunnel direction.

In view of the static disorder of the H_2O molecules, we adopted a split-atom model, where O3 was located at a 4*e* $(0,0,z)$ position with $U(\mathrm{O3})$ refined instead of $U_{ij}(\mathrm{O3})$'s. Such a modification of the structural model significantly decreased $U(\mathrm{O3})$ with negligible changes in *R* factors.

The final *R* factors were quite low: $R_{wp} = 4.56\%$, $R_p = 3.67\%$, $R_B = 1.52\%$, and $R_F = 0.77\%$ with a goodness-of-fit indicator of $S = R_{wp}/R_e = 1.23$. Fig. 2 shows observed, calculated and difference patterns for the Rietveld refinement from the neutron powder diffraction data of $MnO_2 \cdot 0.1(D_{0.34}H_{0.66})_2O$. Lattice parameters were $a = 9.777(2)$ and $c = 2.8548(5)$ Å. The fairly high background is due to the marked incoherent scattering from H atoms. Tables 2 and 3 list the structure parameters of $MnO_2 \cdot 0.1(D_{0.34}H_{0.66})_2O$, and selected interatomic distances and bond angles, respectively.

3.2. Rietveld and MPF analyses from the synchrotron and conventional XRD data

Coefficients for analytical approximations to atomic scattering factors for Mn, O, and H were taken from Ref. [29]. Their anomalous scattering factors were evaluated with a computer program CROMER by the Cromer–Liberman method adopting a Kissel–Pratt correction [30]. Thermal motion was regarded as isotropic for all the sites. Into the Rietveld refinements, we introduced a virtual chemical species, WO, whose atomic scattering factor is the sum of those for one O and two H atoms. Because of a strong correlation between $U(\mathrm{WO})$ and $g(\mathrm{WO})$, $U(\mathrm{WO})$ was fixed at 0.06333 Å^2 assumed for tunnel water in todorokite [13]. WO was located at the ideal 2*b* position without adopting the split-atom model because the fractional coordinate, *z*, for the 4*e* site did not converge in contrast with the Rietveld refinement from the neutron diffraction data.

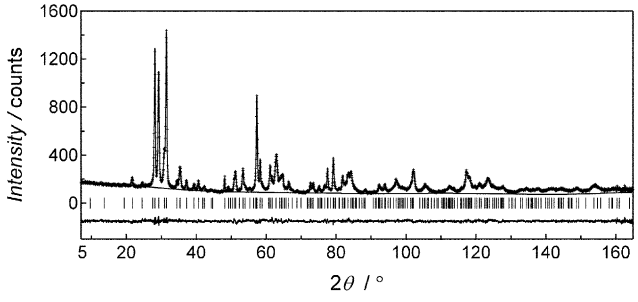

Fig. 2. Observed (plus marks), calculated (solid line), and difference (bottom) patterns for the Rietveld refinement from the neutron diffraction data of $MnO_2 \cdot 0.1(D_{0.34}H_{0.66})_2O$. The short vertical lines below the profiles mark the peak positions of all the possible Bragg reflections.

Fig. 3 exemplifies Rietveld refinement patterns for the synchrotron XRD data in a 2θ range from 31° to 41.5°. Part of reflections in this figure exhibited highly anisotropic profile broadening, which stems from stacking faults along the needle axis (Fig. 1). All the $0\,0\,l$ reflections were sharp, whereas no systematic relations could be found among diffraction indices, $h\,k\,l$, and full-widths at half-maximum. Similar tendencies were also observed in the conventional X-ray and neutron diffraction patterns.

After the refinement of an anisotropy coefficient for strain broadening, U_e, the technique of partial profile relaxation [19,22] was applied to 26 reflections in the synchrotron XRD data and to 18 reflections in the conventional XRD data. Despite the anisotropic profile broadening, partial profile relaxation improved the goodness-of-fit dramatically. For example, R_{wp} decreased from 7.11% to 2.66% for the synchrotron XRD data and from 8.46% to 5.06% for the conventional XRD data as compared with the use of the pseudo-Voigt profile function of Thomson et al. [31] made asymmetric with the procedure of Finger et al. [32]. It should be noted that anisotropy coefficients for

Table 2
Structure parameters of $MnO_2 \cdot 0.1(D_{0.34}H_{0.66})_2O$ determined from the neutron powder diffraction data[a]

Atom	Site	*g*	*n*	*x*	*y*	*z*	U (Å^2)
Mn	8*h*	1	8	0.3467(3)	0.1678(3)	0	
O1	8*h*	1	8	0.1552(3)	0.2029(2)	0	
O2	8*h*	1	8	0.5420(2)	0.1630(3)	0	
O3	4*e*	0.2	0.8	0	0	0.59(2)	0.11(2)
Atom	U_{11}	U_{22}	U_{33}	U_{12}	U_{13}	U_{23}	U_{eq} (Å^2)
Mn	1.17(12)	0.87(13)	0.14(6)	0.12(13)	0	0	0.00730
O1	0.68(11)	1.16(9)	0.38(6)	0.61(8)	0	0	0.00744
O2	0.70(9)	1.02(11)	0.58(5)	0.57(8)	0	0	0.00770

[a] Definitions: *g*, occupation factor; *n*, number of atoms per unit cell; U_{eq}, equivalent isotropic atomic displacement parameter. *U* is the isotropic atomic displacement parameter when the Debye–Waller factor is represented as $\exp(-8\pi^2 U \sin^2\theta/\lambda^2)$. U_{ij}'s are anisotropic atomic displacement parameters (10^{-2} Å^2) when the Debye–Waller factor is represented as $\exp[-2\pi^2(h^2a^{*2}U_{11} + k^2b^{*2}U_{22} + l^2c^{*2}U_{33} + 2hka^*b^*U_{12} + 2hla^*c^*U_{13} + 2klb^*c^*U_{23})]$.

Table 3
Selected interatomic distances, l, and bond angles, ϕ, calculated from the crystal data obtained with the neutron powder diffraction data of $MnO_2 \cdot 0.1(D_{0.34}H_{0.66})_2O$[a]

l (Å)	
Mn–O1	1.903(4)
Mn–O1^{i} × 2	1.906(3)
Mn–O2	1.909(4)
Mn–O2^{ii} × 2	1.886(2)
Mean	1.899
ϕ (deg)	
O1–Mn–O1^{i}	82.5(2)
O1–Mn–O2^{ii}	93.8(2)
O1^{i}–Mn–O2	91.5(2)
O1^{i}–Mn–O2^{ii}	82.24(5)
O2–Mn–O2^{ii}	92.0(2)

[a] Symmetry codes: (i) $1/2-x$, $1/2-y$, $1/2-z$; (ii) $1/2-y$, $-1/2+x$, $1/2+z$.

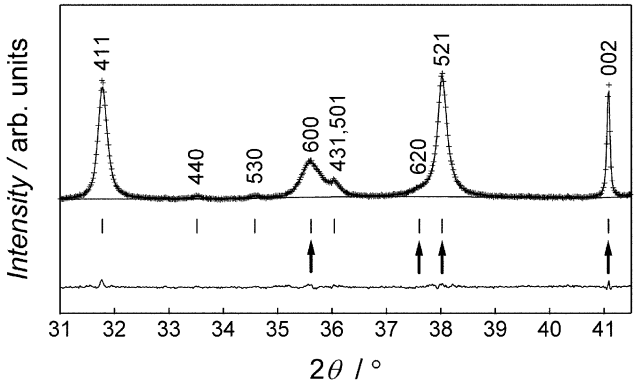

Fig. 3. Part of Rietveld refinement patterns for the synchrotron XRD data of $MnO_2 \cdot 0.15H_2O$. The partial profile relaxation technique was applied to reflections attached with arrows.

Scherrer broadening, X_e, and for strain broadening, Y_e, were also refined in the preliminary refinement using the above combination for representing profile shapes. Partial profile relaxation was most effective in the pattern fitting of our α-MnO_2 specimen because such porous materials often grow to needle crystals showing highly anisotropic profile broadening due to stacking faults along the needle axis. Such a kind of anisotropic profile broadening can hardly be expressed by profile functions with physical meanings.

The resulting R factors reached $R_{wp} = 2.66\%$, $R_p = 2.02\%$, $R_B = 3.02\%$, and $R_F = 1.52\%$ with $S = 1.66$ for the synchrotron XRD data and $R_{wp} = 5.06\%$, $R_p = 3.76\%$, $R_B = 3.16\%$, and $R_F = 1.41\%$ with $S = 1.48$ for the conventional XRD data. Fig. 4 shows observed, calculated, and difference patterns for Rietveld refinements from the synchrotron and conventional XRD data of $MnO_2 \cdot 0.15H_2O$. The lattice parameters

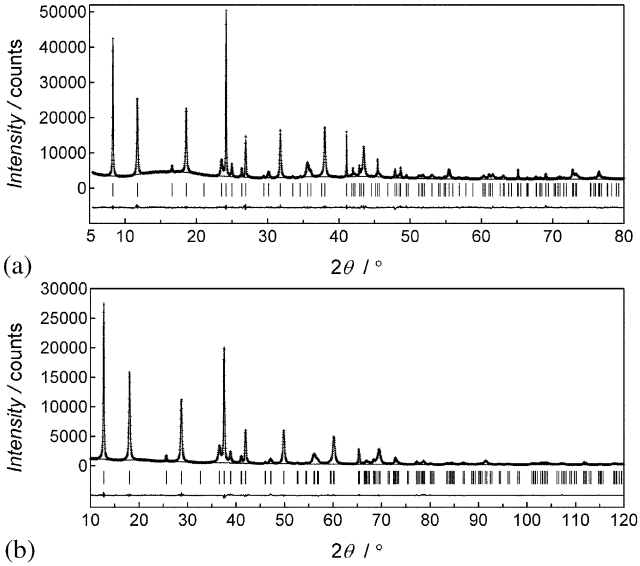

Fig. 4. Observed, calculated, and difference patterns for the Rietveld refinements from the (a) synchrotron and (b) conventional XRD data of $MnO_2 \cdot 0.15H_2O$.

were $a = 9.81359(10)$ and $c = 2.85077(2)$ Å for the synchrotron XRD data, and $a = 9.82304(12)$ and $c = 2.85474(3)$ Å for the conventional XRD data. The wavy background in both diffraction patterns suggests that H_2O molecules are disordered in the tunnel at room temperature. Table 4 lists the final structure parameters of $MnO_2 \cdot 0.15H_2O$.

The Rietveld refinements were followed by MPF to determine electron-density distribution. After two REMEDY cycles, R factors decreased to $R_{wp} = 2.53\%$, $R_p = 1.91\%$, $R_B = 1.19\%$, and $R_F = 0.79\%$ with $S = 1.59$ for the synchrotron XRD data and $R_{wp} = 4.38\%$, $R_p = 3.13\%$, $R_B = 0.72\%$, and $R_F = 0.51\%$ with $S = 1.30$ for the conventional XRD data. The dramatic decreases in R_B and R_F evaluated from 'observed' integrated intensities [1] are particularly noteworthy, reflecting better representation of crystal structures with three-dimensional electron densities in MPF than with structure parameters in the Rietveld analysis. No appreciable differences were noticed between EDD images obtained from the synchrotron and conventional XRD data. This fact is explained in terms of the high ability of MPF to extract structural details even from the medium-resolution XRD data.

4. Discussion

4.1. Framework structure of α-MnO_2

Considerable differences were appreciated among the lattice parameters refined from the different data sets as

Table 4
Structure parameters of $MnO_2 \cdot 0.15H_2O$ determined from the synchrotron and conventional XRD Data

Atom	Site	g	n	x	y	z	U (Å^2)
Synchrotron XRD							
Mn	8*h*	1	8	0.34691(11)	0.16546(13)	0	0.01321(13)
O1	8*h*	1	8	0.1535(3)	0.1994(2)	0	0.0069(3)
O2	8*h*	1	8	0.5389(3)	0.1595(3)	0	$= U$(O1)
WO	2*b*	0.615(6)	1.230(13)	0	0	1/2	0.06333
Conventional XRD							
Mn	8*h*	1	8	0.34800(10)	0.16580(11)	0	0.01023(15)
O1	8*h*	1	8	0.1527(3)	0.1913(2)	0	0.0062(4)
O2	8*h*	1	8	0.5398(2)	0.1614(2)	0	$= U$(O1)
WO	2*b*	0.599(5)	1.198(10)	0	0	1/2	0.06333

listed in Table 1. The lattice parameters of α-MnO_2 were very sensitive to the water content in the tunnel space. As the amount of tunnel water was decreased, a decreased while c hardly changed. This tendency is also reported in the literature [33].

Fig. 5 shows the crystal structure of $MnO_2 \cdot 0.1(D_{0.34}H_{0.66})_2O$ with thermal ellipsoids drawn from the U_{ij}(Mn, O1, and O2) and U(O3) parameters refined in the Rietveld analysis from the neutron diffraction data. As can be appreciated from the Mn–O distances in Table 3, the MnO_6 octahedron is slightly distorted, which has already been pointed out before [12,34]. Mn shifts from the center of the octahedron toward three O2–O2 unshared edges.

To investigate distortion of the MnO_6 octahedron, its quadratic elongation, $\langle\lambda\rangle$, [35] and bond angle variance, σ^2, [35] were calculated with VICS [26]. The quadratic elongation was evaluated using the formula,

$$\langle\lambda\rangle = \sum_{i=1}^{6} \frac{(l_i/l_0)^2}{6}, \quad (1)$$

where l_i is the distance from Mn to ith O, and l_0 is the center-to-vertex distance of a regular octahedron with the same volume. The bond angle variance for the octahedron was calculated with

$$\sigma^2 = \sum_{i=1}^{12} \frac{(\varphi_i - 90^\circ)^2}{11}, \quad (2)$$

where φ_i is the ith bond angle. From the crystal data obtained by the Rietveld refinement from the neutron diffraction data, these parameters were calculated at $\langle\lambda\rangle = 1.011$ and $\sigma^2 = 35.7$ degree^2.

In the case of the MnO_6 octahedron in $Rb_{1.514}Mn_8O_{16}$ having a hollandite-type structure with the large stabilizing cations [34], these parameters were calculated at $\langle\lambda\rangle = 1.013$ and $\sigma^2 = 44.2$ degree^2. The σ^2 value in the Rb-containing compound was somewhat larger than that in the present compound whereas the $\langle\lambda\rangle$ of these two were comparable to each other. The hollandite-type structure distort to be monoclinic ($I2/m$) when stabilizing cations in the tunnel are very small [10,12]. However, α-MnO_2 is still tetragonal ($I4/m$) with the relatively small distortion of the MnO_6 octahedron even if small H_2O molecules are included in the tunnel instead of large stabilizing cations.

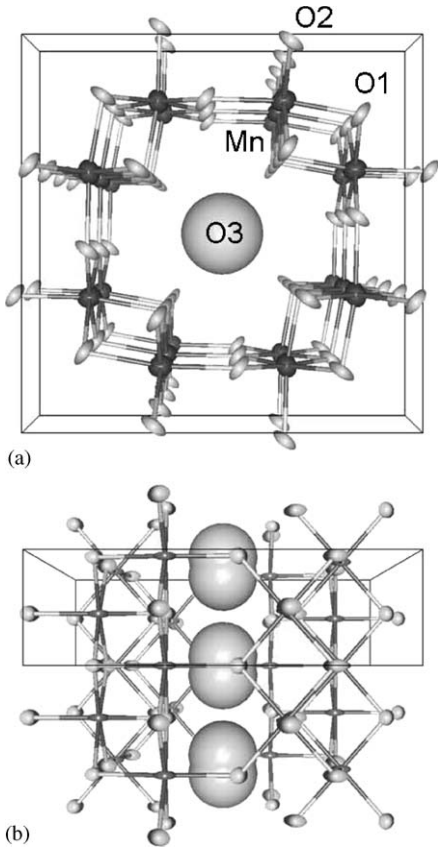

Fig. 5. Structure drawings illustrating thermal ellipsoids in $MnO_2 \cdot 0.1(D_{0.34}H_{0.66})_2O$. Solid boxes indicate the unit cell viewed along the (a) c-axis and (b) a-axis.

4.2. *Oxidation state of* Mn

The bond valence sum [36,37], v, of Mn in the present compound was calculated using the empirical

formula,

$$v = \sum_{i=1}^{6} S_i = \sum_{i=1}^{6} \exp\left(\frac{l_0 - l_i}{0.37}\right), \quad (3)$$

where S_i is the bond valence between Mn and ith O atoms, l_i's are observed Mn–O bond lengths, and l_0 is the bond valence parameter of the Mn^{4+} ion (1.753 Å) [38]. The bond valence sum of Mn was calculated at +4.04 from the Mn–O bond lengths determined from the neutron diffraction data. This v value shows that Mn in our specimen is nearly tetravalent. From the analytical values obtained by the titration and elemental analyses, the mean oxidation state of Mn was estimated to be +3.98, which agrees with the v value within our experimental errors. In addition, if a certain amount of Mn^{3+} ions were contained in α-MnO_2, U_{eq} and U values for the O1 and O2 sites would be larger because of significant local Jahn–Teller distortion. There is no possibility of the existence of Mn^{3+} ions in α-MnO_2 in view of the reasonable values.

4.3. Electron-density distribution

Fig. 6 depicts a structural model and three-dimensional EDD images for $MnO_2 \cdot 0.15H_2O$ obtained by MPF from the synchrotron XRD data. Isosurfaces for number densities of electrons, ρ, were drawn with an equi-density level of $0.3/Å^3$. Fig. 6 supports the idea that the Mn–O bonds have highly covalent character. In fact, $(K, H_3O)_xMn_8O_{16}$ is semiconducting [9]. The minimum ρ value along the line connecting Mn and O atoms is about $0.75/Å^3$. In the MEM analysis of $NdSr_2Mn_2O_7$ [39], the minimum ρ value between Mn and O atoms was reported to be $0.6/Å^3$, which is slightly smaller than those in $MnO_2 \cdot 0.15H_2O$.

In Fig. 6, a faint peak of about $0.6/Å^3$ is visible between O atoms in the rutile-type (1×1) linkage in the hollandite-type structure. The crystal structure of γ-MnOOH is similar to that of β-MnO_2 having a rutile-type structure. However, all the Mn atoms are trivalent, and one-half of the O atoms are replaced by OH^- ions; thus, the H atoms in γ-MnOOH are situated at the rutile-type linkage of MnO_6 octahedra [40]. An attempt to determine the position of such an H/D site in the Rietveld refinement from the neutron diffraction data was unsuccessful. In the present specimen, the existence of OH^- ions seems to be doubtful in view of the oxidation state of Mn very close to +4. This faint peak may be a ghost one.

4.4. Ultramicropore in α-MnO_2

Fig. 7 illustrates two-dimensional EDD maps obtained for (001), (002), and (200) planes in $MnO_2 \cdot 0.15H_2O$ by MPF from the synchrotron XRD data. The

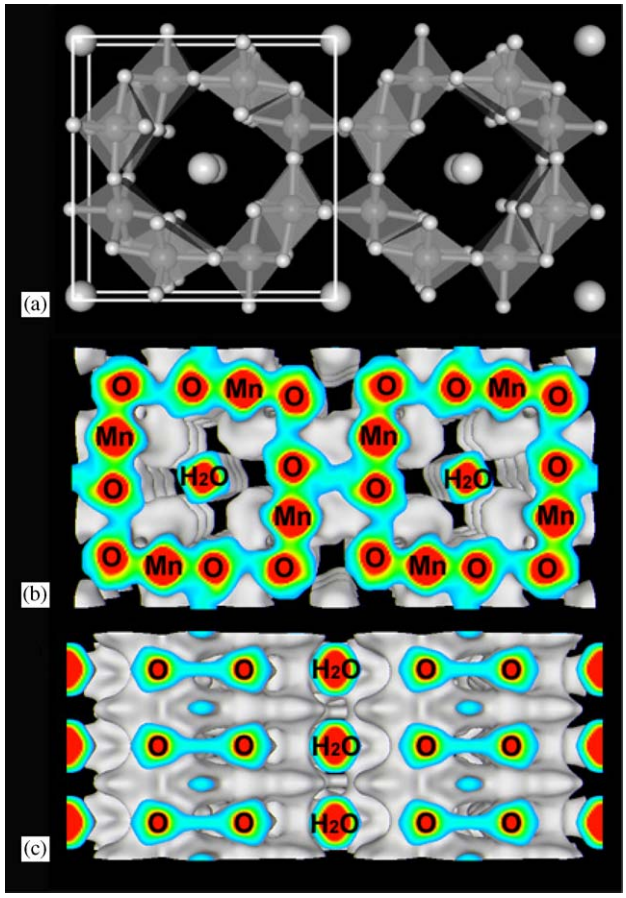

Fig. 6. (a) Crystal structure and three-dimensional EDD images viewed along the (b) [001] and (c) [100] directions for $MnO_2 \cdot 0.15H_2O$. The equi-density level was $0.3/Å^3$. The solid box in (a) indicates the unit cell viewed along the c-axis.

contour lines were plotted only for the lower density region from $0/Å^3$ to $3/Å^3$ with an interval of $0.3/Å^3$. Electron densities were relatively flat below $0.3/Å^3$ and increased abruptly above this level which is, therefore, regarded as 'surface' of the cage. From contour lines for $0.3/Å^3$, the effective inner diameters of the cage in α-MnO_2 are estimated to be about 2.6 Å for a bottleneck on the (002) plane and about 4.8 Å for an inner space on the (001) plane. The pore diameters of the present material are classified as ultramicropores (pore width <7 Å) by definition [41].

Empirical diameters of adsorbable molecules are reported to be 4.3 Å for N_2 at 77 K and 2.2 Å for H_2O at 25°C [42]. The size of the bottleneck (2.6 Å) is much smaller than 4.3 Å for N_2 and larger than 2.2 Å for H_2O. Thus, H_2O molecules can be trapped in the narrow tunnels of α-MnO_2 while N_2 molecules cannot penetrate the tunnel cavity. According to N_2, O_2, H_2O, and NH_3 adsorption isotherms for α-MnO_2 [18,43], only H_2O and NH_3 molecules can be absorbed into the tunnel cavity. These experimental facts are consistent

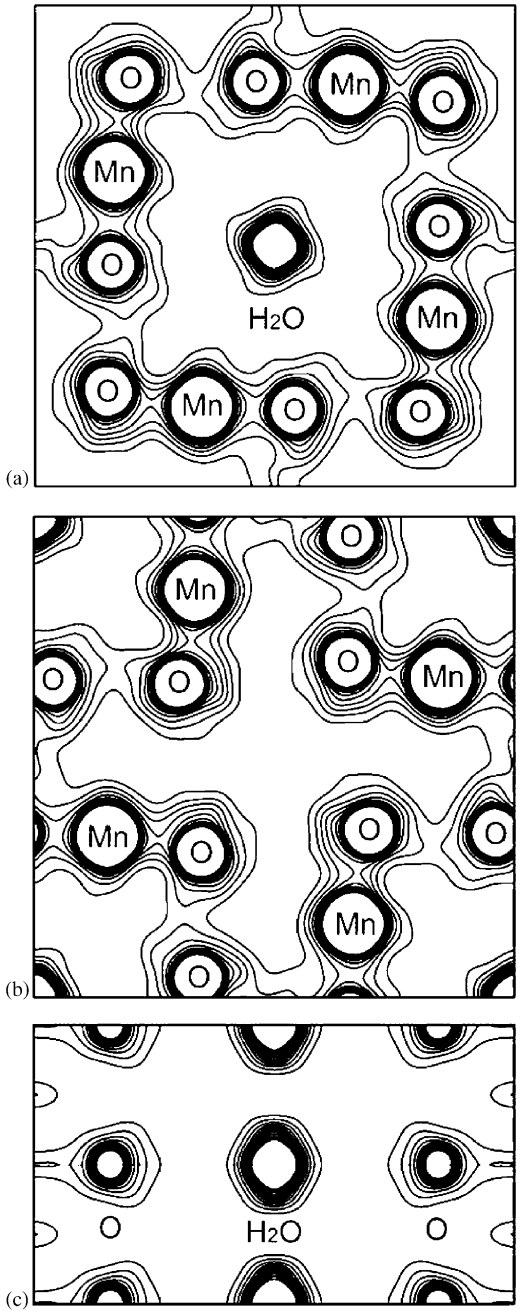

Fig. 7. Two-dimensional EDD maps on the (a) (001), (b) (002), and (c) (200) planes in $MnO_2 \cdot 0.15H_2O$. Contour lines from $0/Å^3$ to $3/Å^3$ were plotted at an interval of $0.3/Å^3$.

with our geometrical estimation from the EDD images, even though the pore diameters obtained in the above manner contain errors in the analysis of EDD.

4.5. Residual water in tunnels

The general formula of α-MnO_2 is represented as $A_x(Mn^{4+}, Mn^{3+})(O^{2-}, OH^-)_2$ ($x = 0$–0.2), where A is a large cation, usually Ba^{2+} (hollandite) or K^+ (cryptomelane) [12]. In our specimen, residual water is accommodated at the A site. From the values of g(WO) refined in the Rietveld refinements from the synchrotron and conventional XRD data, the amount of tunnel water is estimated to be about 0.15 molecules per mol of MnO_2. This value agrees with that obtained by the TG and TPD analysis within experimental errors.

In the case of $Na_xTi_{8-x}Cr_xO_{16}$ with a hollandite-type structure, electron-density maps resulting from MEM analysis offered evidence that small Na^+ ions are distributed widely in the tunnel space [44,45]. On the other hand, electron densities corresponding to tunnel water in α-MnO_2 are concentrated near the center of the cage (Figs. 6 and 7). This finding suggests that H_2O molecules are dominant in the tunnels rather than H_3O^+ ions. The oxidation state of Mn very close to +4 also supports this idea.

The isosurface of ρ values for tunnel water is considerably elongated along the tunnel direction, as Figs. 6 and 7 show. Moreover, the displacement of O3 off the ideal $2b$ site was required in our Rietveld refinement from the neutron diffraction data. These findings show that H_2O molecules are not only vibrating markedly but also highly disordered, particularly along the [001] direction, near the center of the cage.

H_2O molecules occluded within the tunnel can be removed from α-MnO_2 on heat treatment at 300°C without structural destruction; the dehydrated α-MnO_2 specimen has strong affinity for water on exposure to air. Thus, H_2O molecules are trapped in the narrow tunnel with strong adsorption potential due to micropore filling and highly disordered along the tunnel direction.

5. Summary

1. The structure parameters of α-type $MnO_2 \cdot 0.1(D_{0.34}H_{0.66})_2O$ were determined by the Rietveld refinement from the neutron powder diffraction data. In addition, the EDD images in $MnO_2 \cdot 0.15H_2O$ were visualized by MPF from both the synchrotron and conventional XRD data.

2. The calculations of $\langle\lambda\rangle$ and σ^2 for the MnO_6 octahedron showed that the distortion of the MnO_6 octahedron is relatively small even if small H_2O molecules are contained in the tunnels instead of large stabilizing cations.

3. The bond valence sum of Mn in α-MnO_2 was estimated at +4.04, which provides evidence that Mn in our specimen is nearly tetravalent.

4. The inner effective diameters of the cage in α-MnO_2 were estimated from the EDD images. These values are consistent with the experimental facts that H_2O molecules can be trapped in the narrow tunnels of α-MnO_2 whereas N_2 molecules cannot penetrate the tunnel cavity.

5. The isosurface of the ρ values for tunnel water is considerably elongated along the tunnel direction. Further, to obtain the reasonable $U(O3)$ value, O3 had to be split into two pieces at the 4*e* site in the Rietveld refinement from the neutron diffraction data. These findings support the idea that H_2O molecules are not only vibrating markedly but also highly disordered, particularly along the [001] direction, near the center of the cage.

Acknowledgments

We would like to thank M. Okui, N. Yagi, and A. Nisawa for their help in the synchrotron XRD experiment.

References

[1] H.M. Rietveld, J. Appl. Crystallogr. 2 (1969) 65–71.
[2] H.M. Rietveld, in: R.A. Young (Ed.), The Rietveld Method, Oxford University Press, Oxford, 1995 (Chapter 2).
[3] K.D.M. Harris, M. Tremayne, Chem. Mater. 8 (1996) 2554–2570.
[4] J.E. Post, Proc. Natl. Acad. Sci. USA 96 (1999) 3447–3454 and references therein.
[5] A.F. Wells, Structural Inorganic Chemistry, 5th Edition, Clarendon Press, Oxford, 1984, pp. 555–556.
[6] M.M. Thackeray, Prog. Solid State Chem. 25 (1997) 1–71 and references therein.
[7] Q. Feng, H. Kanoh, K. Ooi, J. Mater. Chem. 9 (1999) 319–333 and references therein.
[8] S.L. Brock, N. Duan, Z.R. Tian, O. Giraldo, H. Zhou, S.L. Suib, Chem. Mater. 10 (1998) 2619–2628 and references therein.
[9] P. Strobel, J. Vicat, D.T. Qui, J. Solid State Chem. 55 (1984) 67–73.
[10] J. Vicat, E. Fanchon, P. Strobel, D.T. Qui, Acta Crystallogr. Sect. B 42 (1986) 162–167.
[11] A. Byström, A.M. Byström, Acta Crystallogr. 3 (1950) 146–154.
[12] J.E. Post, R.B. von Dreele, P.R. Buseck, Acta Crystallogr. Sect. B 38 (1982) 1056–1065.
[13] J.E. Post, D.L. Bish, Am. Mineral. 73 (1988) 861–869.
[14] S. Turner, J.E. Post, Am. Mineral. 73 (1988) 1155–1161.
[15] J.E. Post, D.L. Bish, in: D.L. Bish, J.E. Post (Eds.), Modern Powder Diffraction, Mineral. Soc. Am., Washington, DC, 1989 (Chapter 9).
[16] J.E. Post, D.R. Veblen, Am. Mineral. 75 (1990) 477–489.
[17] M.H. Rossouw, D.C. Liles, M.M. Thackeray, Mater. Res. Bull. 27 (1992) 221–230.
[18] N. Kijima, H. Yasuda, T. Sato, Y. Yoshimura, J. Solid State Chem. 159 (2001) 94–102 ERRATUM: J. Solid State Chem. 160, (2001) 292.
[19] F. Izumi, Rigaku J. 17 (2000) 34–45.
[20] F. Izumi, S. Kumazawa, T. Ikeda, W.-Z. Hu, A. Yamamoto, K. Oikawa, Mater. Sci. Forum 378–381 (2001) 59–64.
[21] F. Izumi, R.A. Dilanian, Recent Research Developments in Physics, Vol. 3, Transworld Research Network, Trivandrum, 2002, pp. 699–726.
[22] F. Izumi, T. Ikeda, Mater. Sci. Forum 321–324 (2000) 198–203.
[23] F. Izumi, in: R.A. Young (Ed.), The Rietveld Method, Oxford University Press, Oxford, 1995 (Chapter 13).
[24] H. Toraya, J. Appl. Crystallogr. 23 (1990) 485–491.
[25] L.B. McCusker, R.B. von Dreele, D.E. Cox, D. Louër, P. Scardi, J. Appl. Crystallogr. 32 (1999) 36–50.
[26] R.A. Dilanian, F. Izumi, unpublished work.
[27] V.F. Sears, in: A.J. Wilson, E. Prince (Eds.), International Tables for Crystallography, Vol. C, 2nd Edition, Kluwer Academic Publishers, Dordrecht, 1999, pp. 440–450.
[28] R.A. Young, in: R.A. Young (Ed.), The Rietveld Method, Oxford University Press, Oxford, 1995 (Chapter 1).
[29] E.N. Maslen, A.G. Fox, M.A. O'Keefe, in: A.J. Wilson, E. Prince (Eds.), International Tables for Crystallography, Vol. C, 2nd Edition, Kluwer Academic Publishers, Dordrecht, 1999, pp. 548–584.
[30] L. Kissel, R.H. Pratt, Acta Crystallogr. Sect. A 46 (1990) 170–175.
[31] P. Thompson, D.E. Cox, J.B. Hastings, J. Appl. Crystallogr. 20 (1987) 79–83.
[32] L.W. Finger, D.E. Cox, A.P. Jephcoat, J. Appl. Crystallogr. 27 (1994) 892–900.
[33] C.S. Johnson, D.W. Dees, M.F. Mansuetto, M.M. Thackeray, D.R. Vissers, D. Argyriou, C.-K. Loong, L. Christensec, J. Power Sources 68 (1997) 570–577 ERRATUM: J. Power Sources 75, (1998) 183–184.
[34] N. Yamamoto, Y. Oka, O. Tamada, Mineral. J. 15 (1990) 41–49.
[35] K. Robinson, G.V. Gibbs, P.H. Ribbe, Science 172 (1971) 567–570.
[36] I.D. Brown, R.D. Shannon, Acta Crystallogr. Sect. A 29 (1973) 266–282.
[37] I.D. Brown, D. Altermatt, Acta Crystallogr. Sect. B 41 (1985) 244–247.
[38] N.E. Brese, M. O'Keeffe, Acta Crystallogr. Sect. B 47 (1991) 192–197.
[39] M. Takata, E. Nishibori, K. Kato, M. Sakata, Y. Moritomo, J. Phys. Soc. Jpn. 68 (1999) 2190–2193.
[40] T. Kohler, T. Armbruster, E. Libowitzky, J. Solid State Chem. 133 (1997) 486–500.
[41] K.S.W. Sing, D.H. Everett, R.A.W. Haul, L. Moscou, R.A. Pierotti, J. Rouquėrol, T. Siemieniewska, Pure Appl. Chem. 57 (1985) 603–619.
[42] H. Naono, M. Shimoda, N. Morita, M. Hakuman, K. Nakai, S. Kondo, Langmuir 13 (1997) 1297–1302 and references therein.
[43] Z.-M. Wang, S. Tezuka, H. Kanoh, Chem. Lett. (2000) 560–561.
[44] Y. Michiue, M. Watanabe, Solid State Ionics 79 (1995) 116–119.
[45] Y. Michiue, A. Sato, M. Watanabe, J. Solid State Chem. 145 (1999) 182–185.